DAAM1 stabilizes epithelial junctions by restraining WAVE complex–dependent lateral membrane motility

Tamako Nishimura,[1] Shoko Ito,[1] Hiroko Saito,[1] Sylvain Hiver,[1] Kenta Shigetomi,[2] Junichi Ikenouchi,[2] and Masatoshi Takeichi[1]

[1]RIKEN Center for Developmental Biology, Chuo-ku, Kobe 650-0047, Japan
[2]Department of Biology, Faculty of Sciences, Kyushu University, Nishi-Ku, Fukuoka 819-0395, Japan

Epithelial junctions comprise two subdomains, the apical junctional complex (AJC) and the adjacent lateral membrane contacts (LCs), that span the majority of the junction. The AJC is lined with circumferential actin cables, whereas the LCs are associated with less-organized actin filaments whose roles are elusive. We found that DAAM1, a formin family actin regulator, accumulated at the LCs, and its depletion caused dispersion of actin filaments at these sites while hardly affecting circumferential actin cables. DAAM1 loss enhanced the motility of LC-forming membranes, leading to their invasion of neighboring cell layers, as well as disruption of polarized epithelial layers. We found that components of the WAVE complex and its downstream targets were required for the elevation of LC motility caused by DAAM1 loss. These findings suggest that the LC membranes are motile by nature because of the WAVE complex, but DAAM1-mediated actin regulation normally restrains this motility, thereby stabilizing epithelial architecture, and that DAAM1 loss evokes invasive abilities of epithelial cells.

Introduction

Epithelial cells organize into a polarized two-dimensional sheet. These sheets are normally stable, but their ordered architecture is often disrupted in various pathological processes such as cancer invasion and metastasis. Invasive cancer cells form podosomes or invadopodia from their basal membranes, which allow them to infiltrate into extracellular matrices (Murphy and Courtneidge, 2011). These cells also tend to lose their original polarity and normal cell–cell association (Gupta and Massagué, 2006; Etienne-Manneville, 2008; Yang and Weinberg, 2008). It is thus important to elucidate the mechanisms by which epithelial cells maintain their integrity, including stable cell–cell adhesion.

In simple epithelia, cuboidal or columnar cells attach to each other via their lateral membranes. Adhesion between these membranes is achieved by multiple junctional structures, which include zonula occludens (ZO; also called tight junction [TJ]), zonula adherens (ZA), and macula adherens (desmosome). TJ and ZA are arranged next to each other at the apical-most edge of cell–cell contacts, forming the apical junctional complex (AJC; Farquhar and Palade, 1963; Vogelmann and Nelson, 2005). The AJC is lined with a bundle of actin filaments (F-actin), which is called the "circumferential actin belt or cables." This actin belt functions in a variety of morphogenetic processes, such as apical constriction and intercalation of epithelial cells (Nishimura

et al., 2012; Martin and Goldstein, 2014; Walck-Shannon and Hardin, 2014). The E-cadherin–β-catenin–α-catenin complex (CCC), a major adhesion receptor organizing the ZA, plays a pivotal role in anchoring F-actin to the AJC (Takeichi, 2014). Below the AJC, E-cadherin–positive junctions extend to the basal ends of the cells, organizing the "lateral membrane contacts" (LCs). Although LCs span the majority of the junctions, the structure and function of LCs are not as well characterized as those of AJCs. F-actin accumulates along the LCs, but without forming defined subcellular structures. The role of this population of F-actin remains largely unknown, although previous studies suggest that it is involved in junctional contractility (Wu et al., 2014) or "cadherin flow" in restricted cell types (Kametani and Takeichi, 2007).

Actin polymerization is regulated by several proteins. The formin family is a group of proteins that is involved in linear actin polymerization (Chesarone et al., 2010). Formins bind to the elongating tips of F-actin and sustain its polymerization via their FH2 domain. In some formins, their actin-polymerizing activity is regulated by small G proteins, such as Rho. Another group of actin regulators is the Scar/WAVE regulatory complex (WRC), whose activity depends on Rac (Takenawa and Suetsugu, 2007). When activated by Rac, the WRC in turn activates the Arp2/3 complex, which enables the branching polymerization of actin (Ridley, 2011; Rotty et al.,

2013). An adaptor protein, Lamellipodin, also interacts with the WRC for modulating the action of the latter, as well as for regulating actin polymerization via Ena/VASP proteins (Law et al., 2013). These actin regulators are especially active at the leading edges of cells to promote their migration (Krause and Gautreau, 2014).

Several formins have been reported to be involved in cell–cell adhesion (Kobielak et al., 2004; Carramusa et al., 2007; Grikscheit et al., 2015). DAAM1 (Dishevelled-associated activator of morphogenesis 1) is one such formin, which has been identified as a regulator of cell polarity (Habas et al., 2001; Ang et al., 2010; Ju et al., 2010; Nishimura et al., 2012). DAAM1 interacts with Rho and Dishevelled via its N- and C-terminal region, respectively, so as to be activated (Liu et al., 2008). In the present study, we explored the role of DAAM1 in epithelial junction formation using a mouse mammary gland–derived epithelial cell line, EpH4 (López-Barahona et al., 1995). We found that DAAM1 localizes at the LCs, and it regulates actin assembly at these sites. Our results suggest that the membranes of LCs are motile by nature because of the action of the WRC, but this motility is suppressed by DAAM1, resulting in the stabilization of epithelial architecture.

Results

Distribution of DAAM1 at lateral cell–cell contacts

EpH4 cells show typical epithelial junctions consisting of AJCs and LCs, which associate with linear F-actin cables and amorphous F-actin networks, respectively (Fig. 1, A and B). These groups of F-actin localized at AJCs and LCs are hereafter referred to as apical and lateral F-actin, respectively, when appropriate. In monolayer cultures of EpH4 cells, the LCs formed at a variety of angles to the culture substrate, and the tilted LCs allowed us to view their molecular composition in a direction perpendicular to the cell layers. Double immunofluorescence staining for DAAM1 and F-actin showed that DAAM1 localized at LCs, colocalizing with lateral F-actin, whereas it rarely colocalized with apical F-actin (Fig. 1 A). In vertically oriented LCs, signals for DAAM1 and F-actin often appeared to overlap at apical regions; however, this may be caused by insufficient resolution of the two signals in confocal images. DAAM1 also colocalized with E-cadherin, except at the AJC where this cadherin was slightly up-regulated along with apical F-actin to organize the ZA (Fig. 1 A). To obtain more precise information about the distribution of DAAM1, we observed cells with the super-resolution system of a confocal microscope (Fig. 1 B). DAAM1 essentially did not overlap with apical F-actin or E-cadherin signals, nor did the TJ protein ZO-1, although faint signals of DAAM1 were occasionally detected from the AJC region in some specimens. These results confirmed that DAAM1 mainly localizes at the LC. In addition, we noticed that the levels of DAAM1, F-actin, and E-cadherin tended to increase around the basal edges of LCs.

DAAM1 interacts with the CCC

To determine how DAAM1 localizes to LCs, we performed deletion analysis of DAAM1. We prepared HA-tagged deletion mutants DAAM1-N and -C (Fig. 2 A) and transiently expressed them in EpH4 cells. DAAM1-N localized to cell junctions in a pattern similar to that of full-length DAAM1, whereas

DAAM1-C did not concentrate at cell–cell contacts (Fig. 2 A). Then, we immunoprecipitated HA-tagged DAAM1-N from the lysates of its stable transfectants and analyzed coprecipitated proteins by mass spectrometry (Fig. S1 A). The coprecipitates contained E-cadherin and α-catenin, prompting us to confirm this result. We expressed full-length HA-tagged DAAM1 in EpH4 cells and immunoprecipitated it from a lysate of the transfectants. The results showed that DAAM1 coprecipitated E-cadherin, α-catenin, and β-catenin (Fig. 2 B), suggesting that the CCC is a binding partner for DAAM1. To further confirm this result, we coexpressed HA-tagged DAAM1 and FLAG-tagged E-cadherin in HEK293T cells and performed immunoprecipitation. The results again demonstrated the binding of E-cadherin with DAAM1 (Fig. 2 C). Moreover, endogenous E-cadherin and DAAM1 also coprecipitated together (Fig. 2 D). To determine which components of the CCC bind DAAM1, we assayed the interaction of DAAM1-N with purified GST-tagged E-cadherin cytoplasmic region, α-catenin, or β-catenin and found that only E-cadherin specifically bound DAAM1 (Fig. 2 E).

To test the interaction of DAAM1 with E-cadherin in vivo, we depleted E-cadherin using a specific siRNA in confluent cultures of EpH4 cells. In these cultures, DAAM1 disappeared or was greatly reduced at cell–cell contact sites, even when another class of adhesion molecule, Nectin-1α (Mandai et al., 2015), was concentrated there (Fig. 2 F, arrows). These results suggest that DAAM1 localizes to cell junctions through its binding to E-cadherin.

DAAM1 depletion causes F-actin dispersion and LC deformation

To investigate whether DAAM1 plays any role in LC formation, we depleted (or knocked down; knockdown [KD]) DAAM1 using its specific siRNAs (Fig. S1 B). DAAM1 depletion caused a striking diffusion of F-actin and E-cadherin signals at the LCs (Fig. 3, A and B; and Fig. S1 C), although the E-cadherin level did not change (Fig. S1 B). In wild-type cells, E-cadherin overlapped with F-actin, whereas this relation became unclear after DAAM1 depletion. Simultaneously, the tilt angle of LCs tended to increase, accompanied by cell height reduction, in DAAM1-depleted cells (Fig. 3, A and B). Despite these changes, the apical F-actin and E-cadherin appeared nearly normal, displaying a sharp line along the apical edges, which suggests that the AJC is hardly affected by DAAM1 depletion. To confirm this, we immunostained for the TJ-associated proteins ZO-1 and Par-3, as well as l-afadin, a ZA protein, and found that the apical localization of these proteins was not affected by DAAM1 removal (Fig. S1, D and E). Likewise, the apical distribution of Myosin-IIA, Myosin-IIB and phosphorylated myosin regulatory light chain was not affected in DAAM1-depleted cells (Fig. S1 F). These results support the idea that DAAM1 regulates LCs, but not the AJC. To further confirm this, we prepared a line of EpH4 cells in which the genes for ZO-1 and ZO-2 were doubly removed (Fig. S2 A). As reported previously (Umeda et al., 2006; Fanning et al., 2012), these cells exhibited dramatic changes in AJC organization: they lost TJ, as assessed by diffuse distribution of claudin-3 (Fig. S2 B), also showing a strong up-regulation of F-actin and E-cadherin along the AJC (Fig. S2 C). Despite these changes, the pattern of DAAM1 distribution was not affected (Fig. S2 C). Furthermore, after DAAM1 depletion, LCs of these cells were deformed in a way similar to that observed in control EpH4 cells (Fig. S2 C). These results confirmed that DAAM1 functions independently of AJC organization.
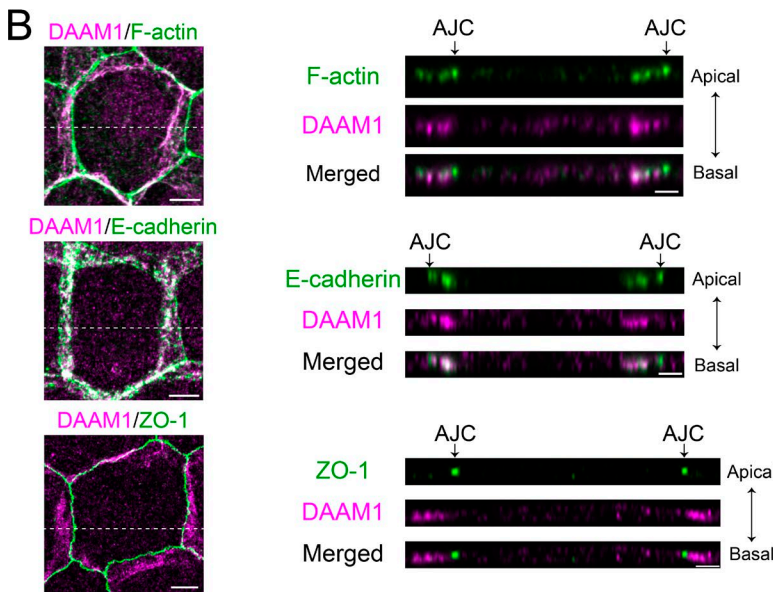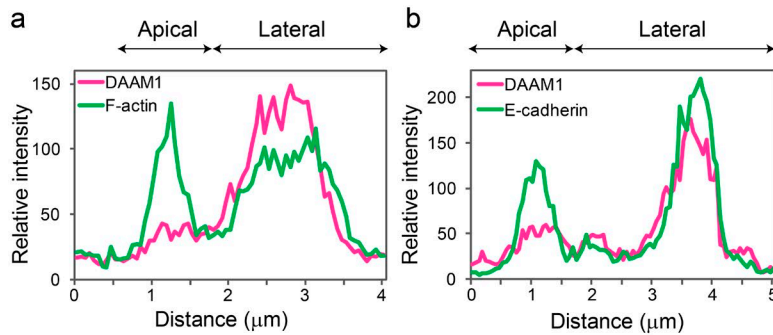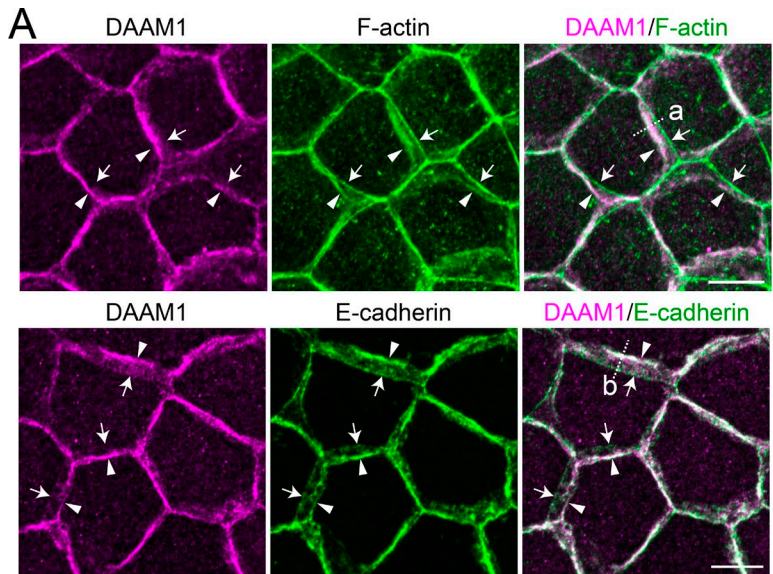
Figure 1. DAAM1 localizes at the lateral contacts in EpH4 cells. (A) Cells were co-stained for DAAM1 and F-actin (top) or E-cadherin (bottom). Z-stack images are shown. Arrows and arrowheads indicate the apical and basal edge, respectively, of cell junctions. Densitometric traces along the dotted lines (a and b) are also shown. Tracing starts from the apical side. (B) Top (left) and lateral (right) views of cells immunostained for the indicated molecules. Z-stacked confocal images were subjected to super-resolution mode processing. The lateral views were taken along the dashed lines. Arrows indicate AJC positions. Bars: (A) 10 μm; (B, top view) 5 μm; (B, lateral view) 2 μm.

For closer analysis of F-actin and E-cadherin behavior at LCs, we transfected EpH4 cells with Lifeact-EGFP to visualize F-actin (Riedl et al., 2008) as well as with E-cadherin–EGFP and acquired their live images. At the LCs of control cells, F-actin was detected as contiguous patches (Fig. 3 C and Video 1). In DAAM1-depleted cells, in contrast, F-actin patches became fragmented into tiny clusters, which vigorously moved around (Fig. 3 C and Video 2). E-cadherin–EGFP was also detected as dynamic clusters at LCs, although their morphological appearance did not differ significantly between control and DAAM1-depleted cells, probably because of the overexpression of this molecule. E-cadherin labeling additionally allowed us to visualize the basal edges of LCs, and we found that the basal edges deformed more dynamically in DAAM1-depleted cells than in controls (Fig. 3 D and Videos 3 and 4). These results suggest that DAAM1 functions to restrain the motility of the cell membranes at LCs.

To test whether the action of DAAM1 depends on its actin-polymerizing activity, we introduced a point mutation of I to A at
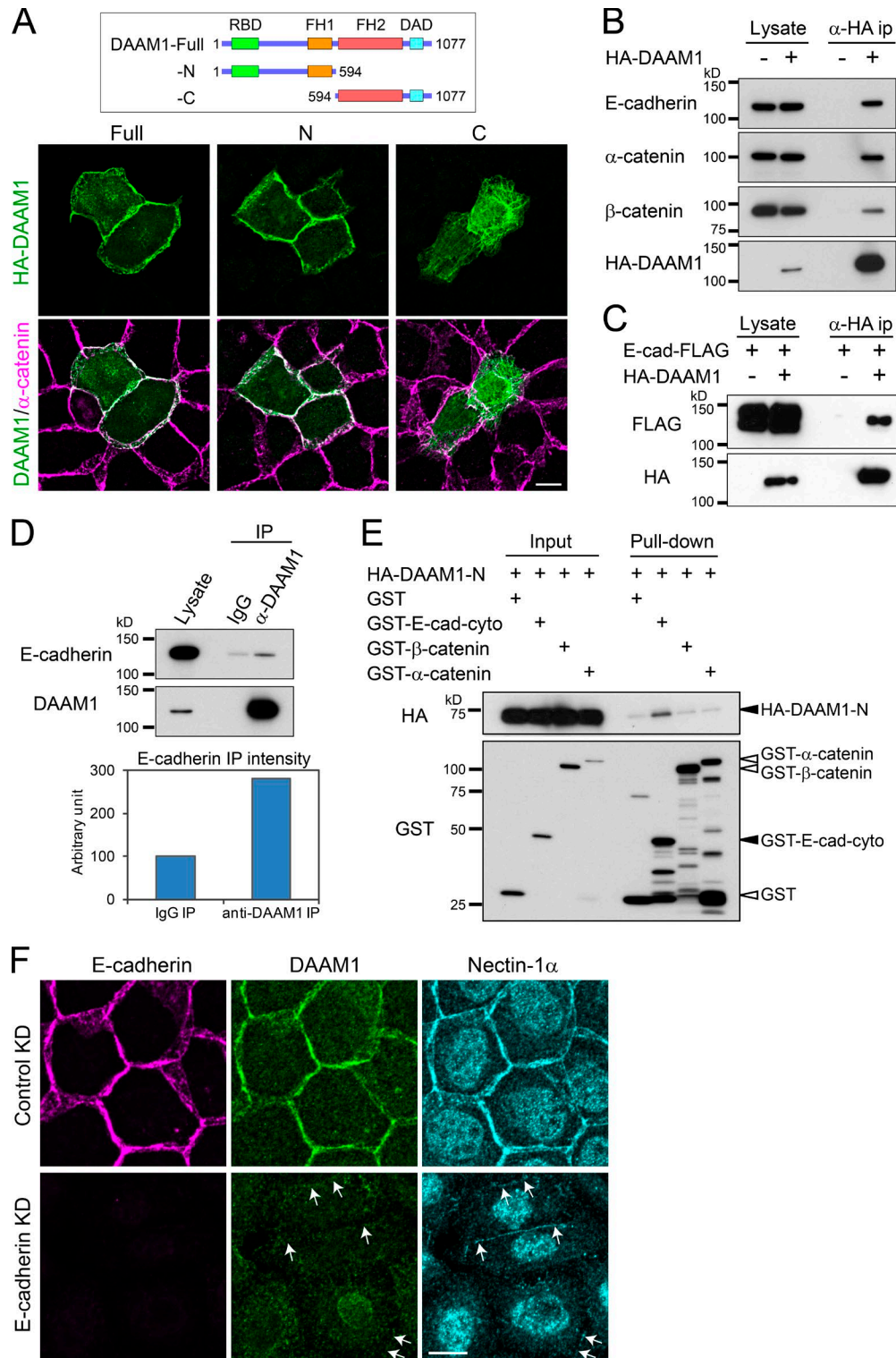
Figure 2. **DAAM1 interacts with the CCC.** (A) DAAM1 localizes at cell contacts via its N-terminal region. (Top) Schematic representation of the deletion mutants of DAAM1. (Bottom) HA-tagged full-length or deletion mutants of DAAM1 were transiently expressed in EpH4 cells and immunostained for HA and α-catenin. (B) Interaction of DAAM1 with the endogenous CCC. Lysates of HA-tagged DAAM1-expressing or parental EpH4 cells were subjected to immunoprecipitation with anti-HA antibody, followed by immunoblotting with antibodies against E-cadherin, α-catenin, β-catenin, or HA. (C) Interaction of DAAM1 with E-cadherin. HEK293T cells were transfected with FLAG-tagged E-cadherin with or without HA-tagged DAAM1. Cell lysates were subjected to immunoprecipitation using anti-HA antibody, followed by immunoblotting with antibodies against FLAG or HA. (D) Interaction between endogenous DAAM1 and E-cadherin. EpH4 cell lysates were subjected to immunoprecipitation by anti-DAAM1 antibody or normal rabbit IgG, followed by immunoblotting with anti–E-cadherin antibody. (E) Interaction of DAAM1-N with the cytoplasmic region of E-cadherin (E-cad–cyto). Lysates of EpH4 cells expressing DAAM1-N were incubated with purified GST-tagged proteins as indicated and subjected to pull-down assays. Note that only GST–E-cad–cyto specifically interacted with DAAM1-N. (F) Distribution of DAAM1 to cell junctions depends on E-cadherin. EpH4 cells were treated with an E-cadherin–specific siRNA for 2 d and then immunostained. Arrows indicate Nectin-1α–positive cell–cell contacts in E-cadherin–depleted cells. (A and F) Bars, 10 μm.
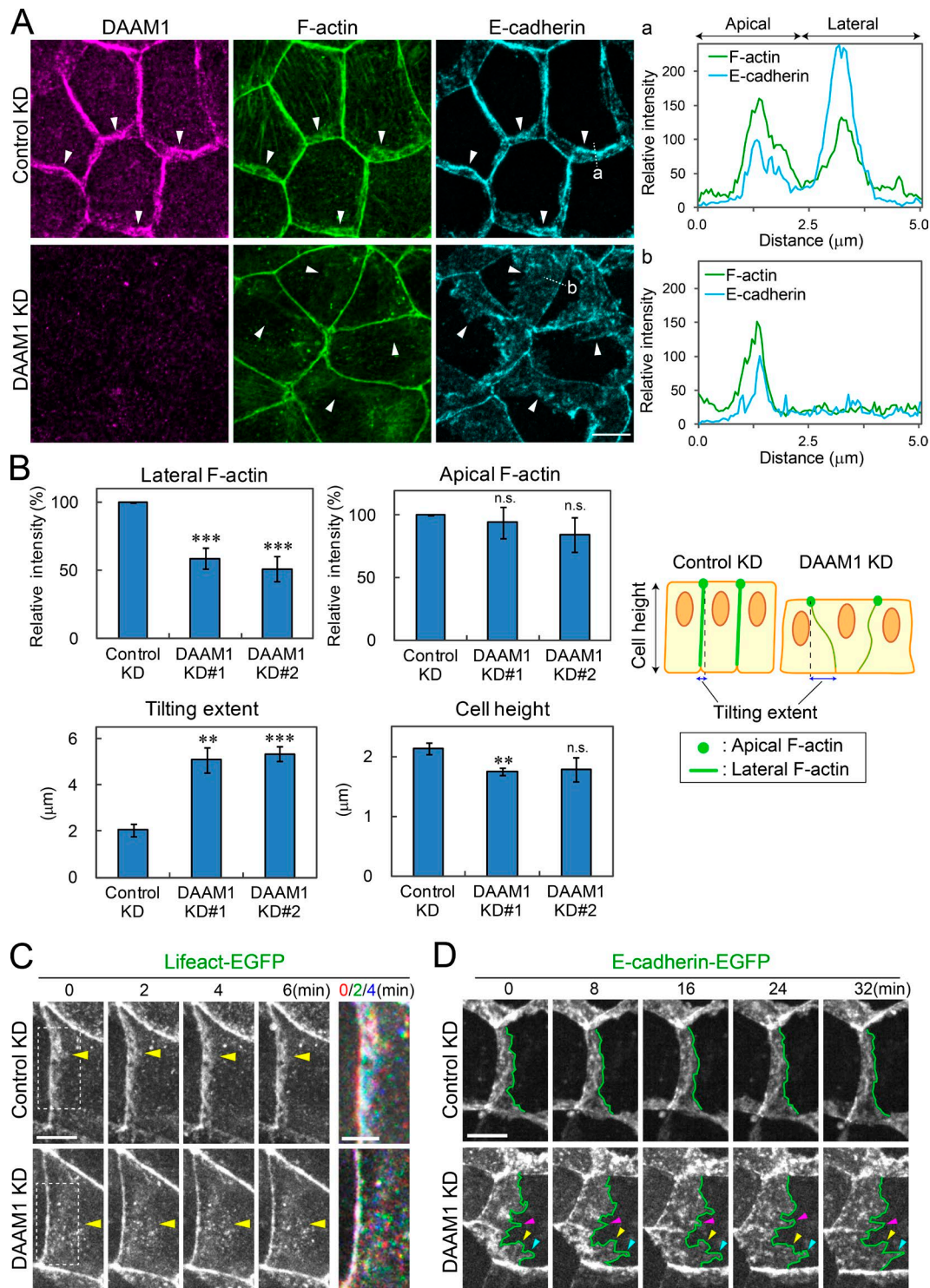
Figure 3. **DAAM1 depletion causes dispersion of lateral F-actin and E-cadherin, not affecting their apical moieties.** (A) EpH4 cells were transfected with DAAM1 siRNA (DAAM1 KD) or control siRNA (Control KD) for 3 d and co-stained for E-cadherin and F-actin. DAAM1 depletion caused dispersion of F-actin and E-cadherin at LCs without affecting their apical distribution. Densitometric traces were performed along the dotted lines (a and b) in an apical to basal direction. Arrowheads point to the basal edges of the junctions. (B) Quantification of apical and lateral F-actin intensity (top), as well as tilting extent of LCs and cell height (bottom), which are defined in the diagram at the right and also in Materials and methods. Histograms represent the mean of three experiments. In each experiment, 50–100 junctions were examined. Two independent DAAM1 siRNAs (KD#1 and #2) were used. Error bars indicate SD. **, $P < 0.01$; ***, $P < 0.001$; n.s., not significant. (C) Still images of Videos 1 and 2 taken for Lifeact-EGFP at the indicated intervals. On the right, the images at 0, 2, and 4 min are merged after coloring Lifeact-EGFP signals red, green, and blue, respectively. The boxed portion is enlarged for the merged images. Note that the majority of F-actin clusters change their positions every 2 min, especially in DAAM1-depleted cells. Yellow arrowheads point to the basal edges of the junctions. (D) Still images of Videos 3 and 4 taken for E-cadherin–EGFP at the indicated intervals. Note that the basal edges, outlined in green, move more dynamically in DAAM1-depleted cells than in controls. Blue, yellow, and pink arrowheads indicate the basal edge of the junction at different points. Bars: (A, C [left], and D) 10 µm; (C, right) 5 µm.
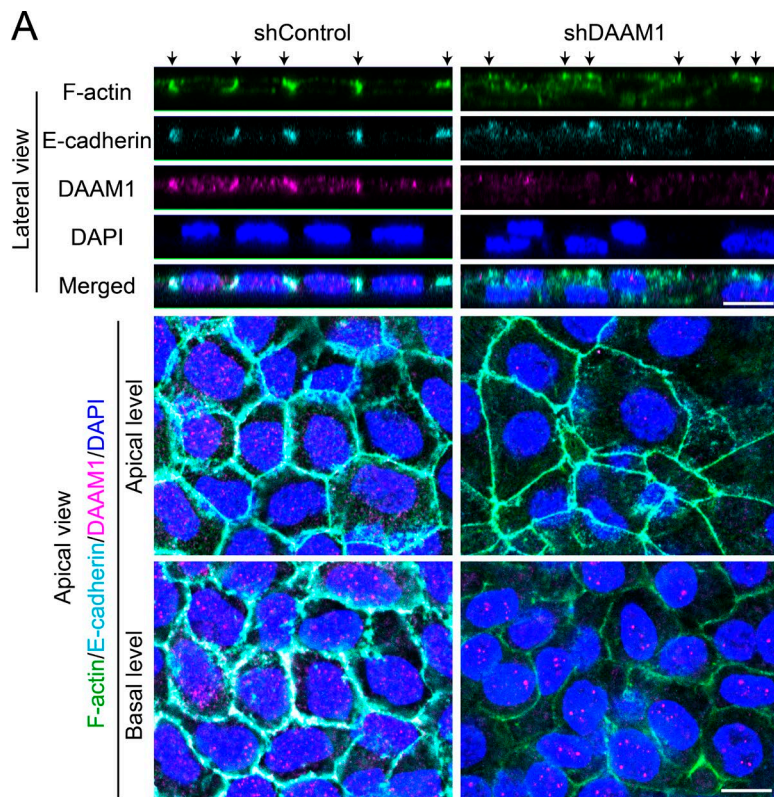
Figure 4. **DAAM1 is important for epithelial integrity.** (A) EpH4 cells stably expressing DAAM1-specific (shDAAM1-1 cells) or control (shControl cells) shRNA were cultured for 2 wk in Transwells and stained for the indicated molecules. (Top) Lateral views. Nuclei are mispositioned in DAAM1-depleted cells. (Bottom) Top views focused on an apical or basal focal plane. Abnormally large or small apical areas are detectable. Arrows indicate AJC positions. Bars, 10 µm. (B) Distribution of the apical area in shControl and shDAAM1 cells. Apical area was defined as the area encircled by ZO-1 immunostaining. 144 shControl and 80 shDAAM1 cells from three and four microscopic fields, respectively, were examined. (C) Rescue of the DAAM1 depletion phenotypes. shDAAM1 cells were additionally transfected with RNAi-resistant EGFP-DAAM1 plasmid and cultured for 2 wk in Transwells; the apical area variation was quantified. We examined 35–144 cells from three or four microscopic fields for each experiment. Histograms represent the mean of three experiments. Error bars indicate SD. *, $P < 0.05$; **, $P < 0.01$; ***, $P < 0.001$.
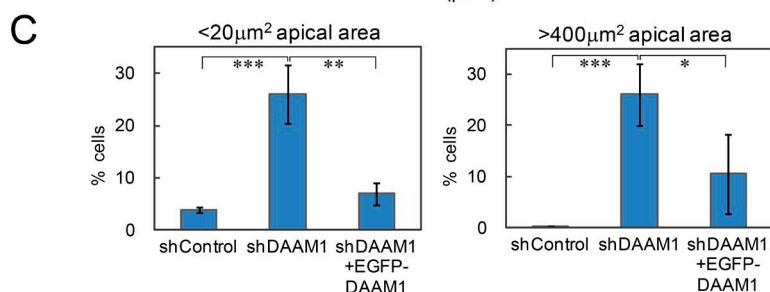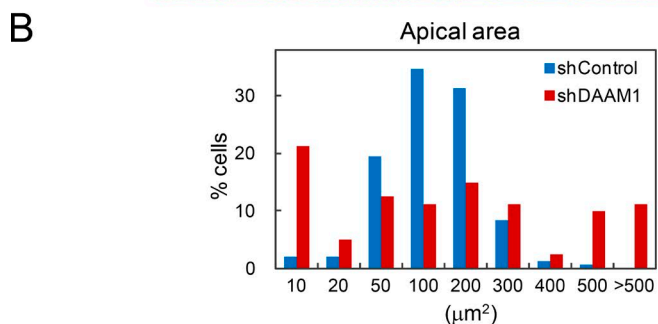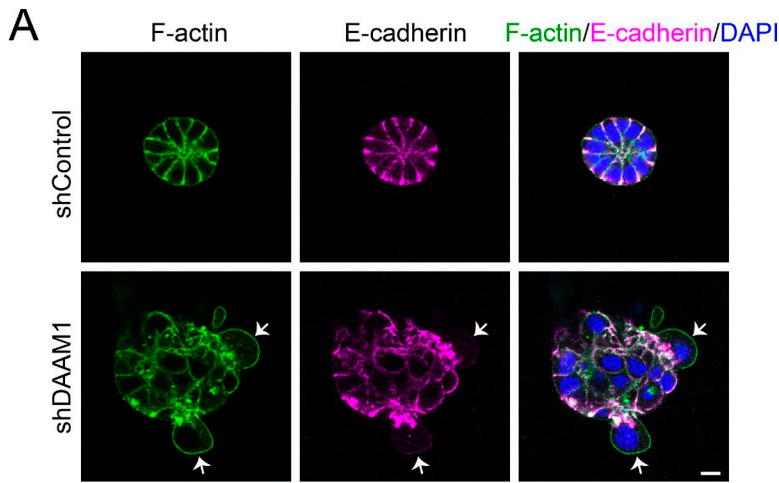
aa698 into this protein, which is known to abolish its actin polymerization activity (Jaiswal et al., 2013). We generated an siRNA-resistant DAAM1 construct for this mutant (DAAM1-I698A), as well as a corresponding wild-type DAAM1. Although the wild-type construct rescued all the DAAM1 KD phenotypes, DAAM1-I698A did not (Fig. S3, A and B), confirming that DAAM1 serves LC stability via its ability to regulate actin polymerization.

DAAM1 is important for preserving epithelial architecture

To further investigate the role of DAAM1 in the formation of epithelial architecture, we established KD cell lines, which stably

express shRNA specific for DAAM1 (shDAAM1) or control shRNA (shControl; Fig. S4 A), and cultured them in Transwell plates, which allow the cells to grow into mature epithelial sheets. At 2 wk, control cells formed a typical monolayer sheet. In DAAM1-depleted cell layers, however, the apical morphology of cells became severely distorted with an increased heterogeneity of the apical surfaces (Fig. 4, A and B). Furthermore, in these cells, nuclei became irregularly arranged, appearing as if the cells were piled up. These abnormities were rescued by expressing an RNAi-resistant EGFP-DAAM1 (Fig. 4 C). These results suggest that DAAM1-deficient cells cannot maintain normal epithelial architecture in long-term cultures.

A

	F-actin	E-cadherin	F-actin/E-cadherin/DAPI

shControl

shDAAM1

B

Spheres with cell extrusion

Average extrusion number

Severe deformation of cells might promote other pathological behaviors. To explore this possibility, we cultured EpH4 cells in Matrigel to allow them to grow into spherical cysts. Control cells formed typical epithelial cysts in which cells were arranged radially (Fig. 5 A). In contrast, DAAM1-depleted cell spheres lost such an ordered arrangement of cells, frequently extruding a fraction of cells from their main body toward the matrix (Fig. 5, A and B). These results further confirmed that DAAM1 is important in maintaining epithelial integrity.

DAAM1 depletion promotes cell edge protrusion

To investigate the abnormal behavior of DAAM1-depleted cells at the cellular level, we transfected shControl or shDAAM1 cells with a membrane-bound EGFP and cultured them on collagen gels. By applying a low transfection efficiency recipe, we obtained confluent cultures in which a labeled cell was surrounded by nonlabeled cells. Live imaging of EGFP in these cells showed that DAAM1-depleted cell lines actively extended protrusions from their basolateral sides, whereas control cells were quiescent (Fig. 6, A and B; and Videos 5 and 6).

To examine whether the increased motility of DAAM1-depleted cells occurred cell-autonomously, we prepared homologous or heterologous mixtures of shDAAM1 and shControl cells, in which either population was labeled with the fluorescent dye CMTPX (Hogan et al., 2009) before mixing. Strikingly, DAAM1-depleted cells extended longer protrusions into neighboring layers when surrounded by control cells than by homologous cells (Fig. 6, C and D), suggesting that the protrusion from DAAM1-depleted cells is enhanced by adjacent wild-type cells. As E-cadherin is detectable along the protrusions, this enhancement appeared to occur at the interface between the surfaces of wild-type and DAAM1-depleted cells.

These findings, together with those shown in Fig. 5, suggest that DAAM1 depletion promotes cell extrusion, particularly when DAAM1-depleted cells are surrounded by normal cells.

Rac-WAVE2 signals enhances LC motility

We asked how the membranes of LCs acquired enhanced motility after DAAM1 depletion. The small GTPase Rac is known to be important for the motile ability of cell edges (Ridley, 2011). We therefore asked whether Rac is involved in LC motility. We treated DAAM1-depleted cells with the Rac inhibitor EHT-1864 and found that the dispersed distribution of E-cadherin was abolished in the treated cells (Fig. S4 B). Live imaging of E-cadherin–EGFP confirmed that the basal edge motility of LCs was almost completely inhibited by EHT-1864 treatment (Video 7). Conversely, when a constitutively active Rac1 (HA-Rac1-G12V) was transiently expressed in control EpH4 cells, the transfected cells broadly extended their LCs under adjacent untransfected cells, being accompanied by a reduction of their apical surface area, even in the presence of DAAM1 (Fig. S4 C), confirming that Rac mediates the deformation of LCs. We then measured Rac activity by pull-down assays but did not find any changes in its activity after DAAM1 KD (Fig. S4 D). These results suggest that DAAM1 does not simply repress Rac activity but may interfere with processes downstream of Rac.

Then, we sought molecules acting downstream of Rac. As the WRC is a well-known Rac effector, we explored whether this complex regulates LC motility. Among the multiple components of the WRC, we focused on WAVE2, as this subtype of WAVE proteins has been shown to be involved in epithelial adhesion (Yamazaki et al., 2007; Verma et al., 2012). WAVE2 localized at LCs overlapping with F-actin clusters, although close analysis of WAVE2 and DAAM1 distributions revealed that many of their immune signals did not overlap with one another
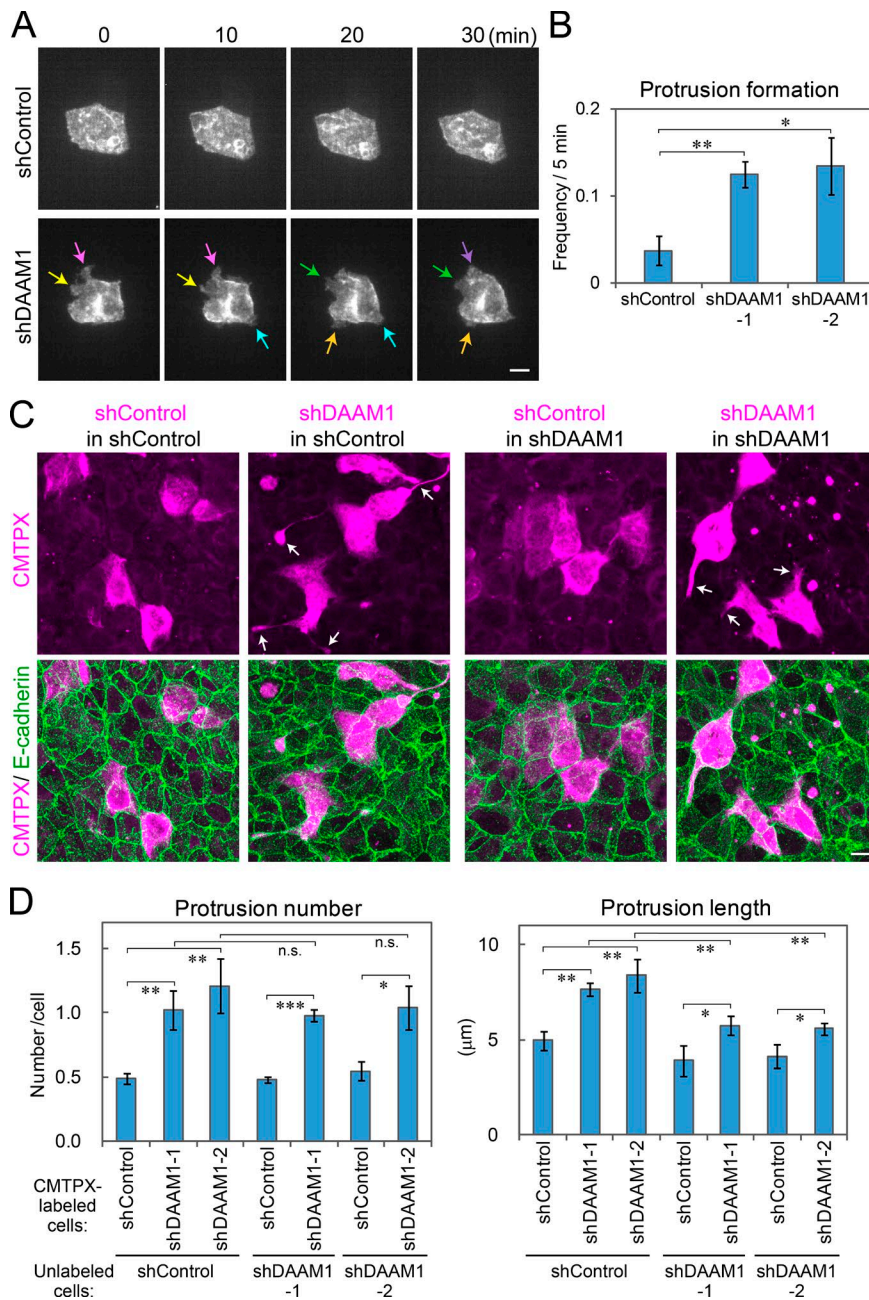
Figure 6. **DAAM1 depletion promotes protrusion of cell edges.** (A) Live imaging of membrane-EGFP introduced into shControl or shDAAM1 cells in confluent cultures. Cells were transfected with membrane-EGFP, leaving the majority of them untransfected, and cultured for 1 d on collagen gels. Representative still images were chosen from Video 5 (for shControl) and Video 6 (for shDAAM1). The labeled cell is surrounded with nonlabeled cells. Arrows indicate representative protrusions. The results obtained using the shDAAM1-2 line are shown. (B) Quantification of the frequency of protrusion per 5 min in two independent lines of shDAAM1 cells or an shControl line. 6–21 cells were examined for each experiment. (C) Mixed cultures of shControl or shDAAM1 cells. Cells were labeled with CMTPX and mixed with nonlabeled cells to culture on collagen gels for 2 d. shDAAM1 cells form longer and more protrusions than shControl cells, especially when mixed with control cells. Arrows indicate representative protrusions. The results obtained using the shDAAM1-2 line are shown. (A and C) Bars, 10 µm. (D) Quantification of protrusion number and length in CMTPX-labeled cells as indicated in Materials and methods. (B and D) Histograms represent the mean of three experiments. Error bars indicate SD. *, $P < 0.05$; **, $P < 0.01$; ***, $P < 0.001$; n.s., not significant.

(Fig. 7 A). In contrast, WAVE2 strongly colocalized with other components of the WRC, including Nap1 and Abi1 (Fig. S4 E), consistent with the model in which they form a complex. These observations suggest that DAAM1 and the WRC organize distinct microdomains. In DAAM1-depleted cells, WAVE2 remained at LCs, partly colocalizing with diffuse F-actin signals especially around the basal regions of LCs (Fig. 7 A).

Then, we knocked down WAVE2 and examined its effects on the phenotypes of DAAM1-depleted cells, using E-cadherin–immunostained samples. WAVE2 depletion in wild-type cells hardly affected junction morphology. When both DAAM1 and WAVE2 were depleted together (Fig. S4 F), the irregular tilting of LCs induced by DAAM1 KD was abolished (Fig. 7, B and C). E-cadherin–EGFP live imaging also confirmed that WAVE2 depletion suppressed the dynamic deformation of LC edges caused by DAAM1 KD (Video 8). We also examined the effect of WAVE2 KD on the protrusion formation by

DAAM1-depleted cells mixed with wild-type cells and found that WAVE2 KD effectively abolished this process (Fig. 7, D and E; and Fig. S4 G). These results suggest that WAVE2 has the ability to promote LC motility, but this ability is suppressed by DAAM1. As WAVE is regulated by phosphorylation at several sites (Mendoza et al., 2011), we tested the effect of DAAM1 depletion on the phosphorylation of WAVE2 at Y150, a site that is phosphorylated by Abl to activate the WAVE2 complex (Leng et al., 2005). However, we did not detect any changes in the level of the phosphorylation (Fig. S4 H).

The WRC cooperates with lamellipodin and Arp2/3 at LCs

Next, we explored which molecules work together with the WRC, focusing on two candidates, lamellipodin and the Arp2/3 complex, that are known to interact with the WRC in Rac-dependent manners (Krause and Gautreau, 2014). Lamellipodin
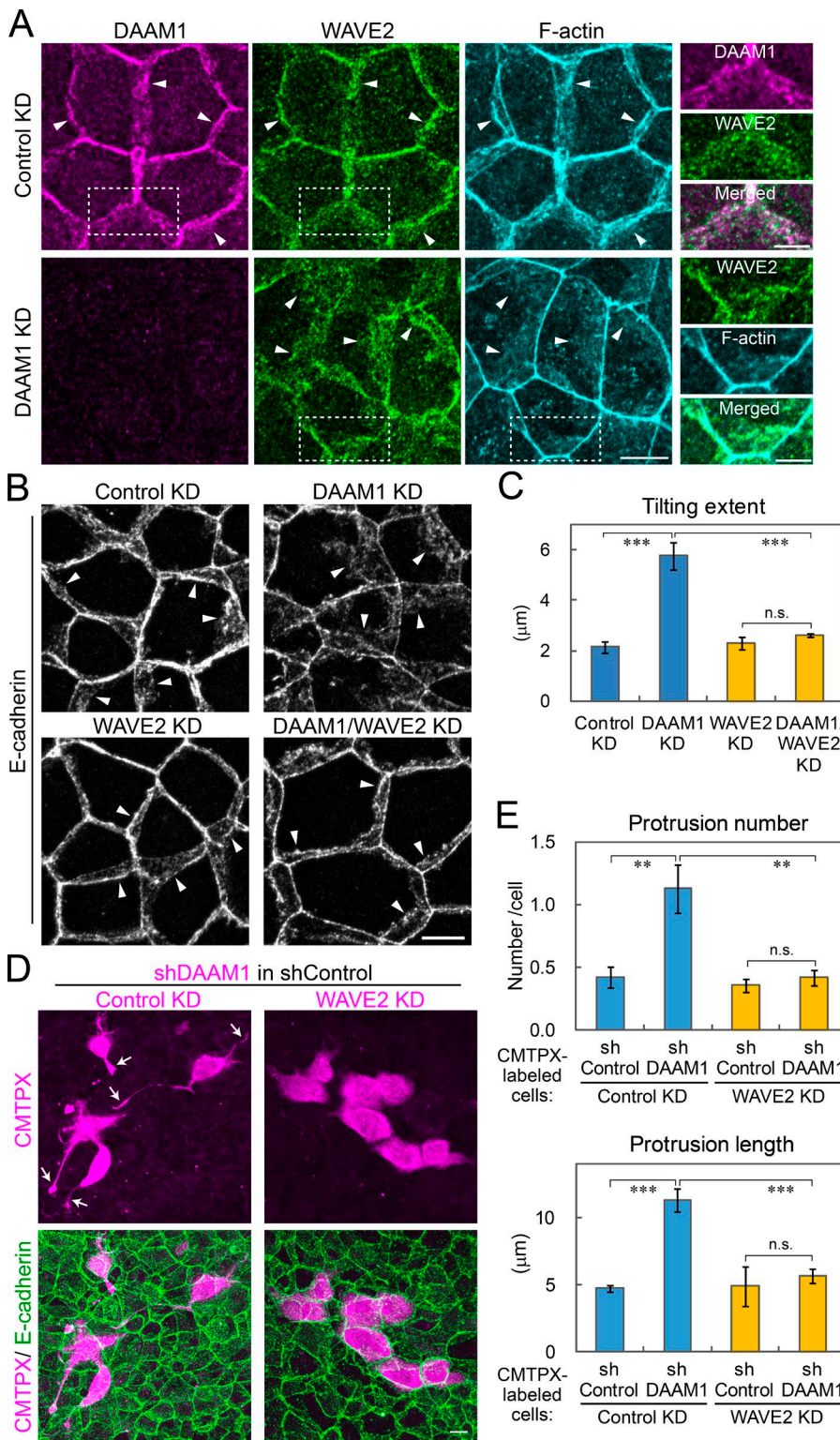
Figure 7. **WAVE2 is required for lateral membrane motility.** (A) Co-staining for DAAM1, WAVE2, and F-actin in EpH4 cells treated with control or DAAM1 siRNA. Enlarged views of the boxed regions are shown at the right. DAAM1 and WAVE2 showed distinct distributions, and WAVE2 overlapped with F-actin. (B) Immunostaining for E-cadherin in EpH4 cells treated with DAAM1 and/or WAVE2 siRNAs. WAVE2 KD tended to cause the sharpening of E-cadherin signals at the basal edges of LCs in both control and DAAM1-depleted cells. (A and B) Arrowheads point to the basal edges of the junctions. (C) Quantification of the tilting extent of LCs. (D) DAAM1-depleted cells were treated with control or WAVE2 siRNAs for 1 d and then labeled with CMTPX. After mixing them with nonlabeled shControl cells, they were cultured on collagen gels for 2 d. Protrusion in DAAM1-depleted cells was suppressed by WAVE2 KD. Arrows indicate representative protrusions. Bars: (A [left], B, and D) 10 µm; (A, right) 5 µm. (E) Quantification of protrusion number and length in the experiment shown in D. (C and E) Histograms represent the mean of three experiments. Error bars indicate SD. **, $P < 0.01$; ***, $P < 0.001$; n.s., not significant.

localized at cell junctions in both control and DAAM1-depleted cells, overlapping with lateral F-actin (Fig. 8 A), as well as with Abi1, a WRC component (Fig. 8 B). Although lamellipodin KD hardly affected junction morphology in wild-type cells, codepletion of lamellipodin and DAAM1 rescued the DAAM1 depletion phenotypes at least in part (Fig. 8, C and D; and Fig. S5 A). This suggests that lamellipodin is involved in the DAAM1 depletion–dependent enhancement of LC motility, likely as a

functional partner of the WRC (Law et al., 2013). Then, we turned our analysis to Arp2/3. Treatment of cells with an Arp2/3 inhibitor, CK-666, showed that it suppresses the DAAM1 KD–induced tilting of LCs, suggesting that Arp2/3 also works in this process. However, depletion of ArpC3, a component of the Arp2/3 complex, disrupted the junctional integrity even in wild-type cells and did not rescue the DAAM1 depletion phenotypes (Fig. S5, B and C), suggesting that the Arp2/3 complex
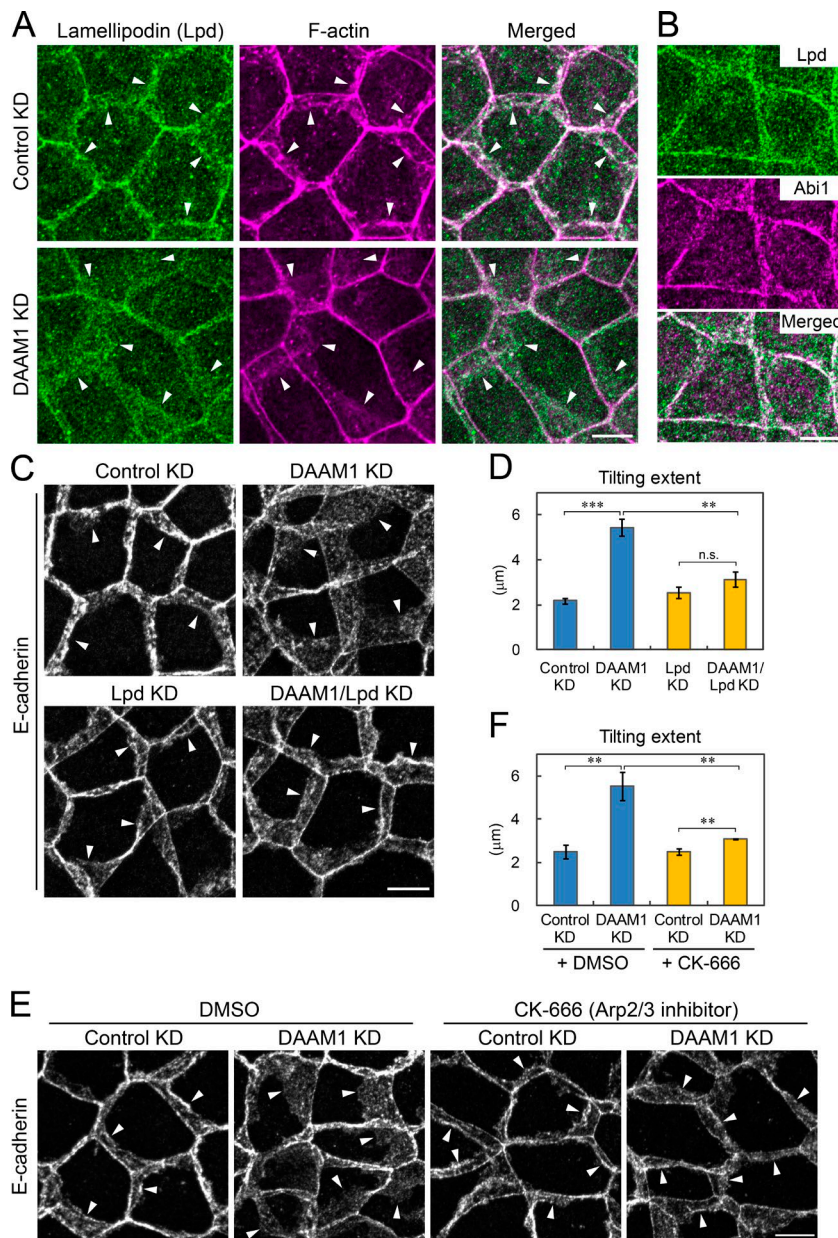
Figure 8. **Lamellipodin and Arp2/3 are involved in lateral membrane motility.** (A) Co-staining for lamellipodin (Lpd) and F-actin in EpH4 cells treated with control or DAAM1 siRNA. Lpd overlapped with F-actin at LCs. (B) Co-staining for Lpd and Abi1. (C) Immunostaining for E-cadherin in EpH4 cells treated with DAAM1 and/or Lpd siRNAs. Depletion of Lpd suppressed the diffused distribution of E-cadherin induced by DAAM1 KD. (D) Quantification of the tilting extent in C. (E) Immunostaining for E-cadherin in control or DAAM1-depleted EpH4 cells treated with 150 µM of the Arp2/3 inhibitor CK-666 in DMSO or DMSO only (0.15% in final concentration) for 30 min. Diffused distribution of E-cadherin induced by DAAM1 KD was partially suppressed. (A–C and E) Arrowheads point to the basal edges of the junctions. Bars, 10 µm. (F) Quantification of the tilting extent in E. (D and F) Histograms represent the mean of three experiments. Error bars indicate SD. **, $P < 0.01$; ***, $P < 0.001$; n.s., not significant.

is fundamentally important to maintain epithelial junctions, in accord with previous observations (Verma et al., 2004, 2012). Thus, it appears that both Arp2/3 and lamellipodin work with the WRC, although the role of Arp2/3 is not restricted to the WRC-dependent regulation of LCs.

RhoA may act upstream of DAAM1 at LCs
Finally, we attempted to characterize signals upstream of DAAM1. In contrast with the Rac-WAVE signaling system, DAAM1 is activated by RhoA, B, or C (Higashi et al., 2008; Liu et al., 2008). Immunostaining for RhoA showed that this molecule localized at cell junctions overlapping with DAAM1 (Fig. 9 A). When RhoA was depleted (Fig. S5 D), lateral F-actin and E-cadherin became diffuse (Fig. 9 B and Fig. S5 E), as found in DAAM1-depleted cells, although DAAM1 signals were not affected in the RhoA-depleted cells (Fig. 9 A). In contrast with DAAM1 depletion, however, the apical F-actin level also tended to decrease (Fig. 9, B and D; and Fig. S5 E). Consistently, live imaging of Lifeact-EGFP indicated that RhoA

depletion induced not only the fragmentation of lateral F-actin but also the disturbance of apical F-actin dynamics. Compared with the rather static appearance of apical F-actin cables in control or DAAM1-depleted cells (Videos 1 and 2), these cables became unstable in RhoA-depleted cells, reorganizing into irregular clusters whose positions changed minute by minute (Fig. 9 E and Video 9). E-cadherin–EGFP signals were also unstable not only at the LCs but also at the AJC in RhoA-depleted cells (Video 10). These results suggest that RhoA controls both LCs and the AJC.

To test whether RhoA regulates DAAM1, we constructed a constitutively active form of DAAM1, DAAM1-ΔDAD, which lacks the C-terminal DAD domain that functions to autoinhibit RhoA binding to the N-terminal domain (Liu et al., 2008). When DAAM1-ΔDAD was expressed in EpH4 cells, it localized to LCs (Fig. 9 C) and suppressed the RhoA loss–dependent dispersion of lateral F-actin and E-cadherin (Fig. 9, B and D). Importantly, however, DAAM1-ΔDAD expression did not rescue the apical RhoA depletion phenotypes (Fig. 9, B and
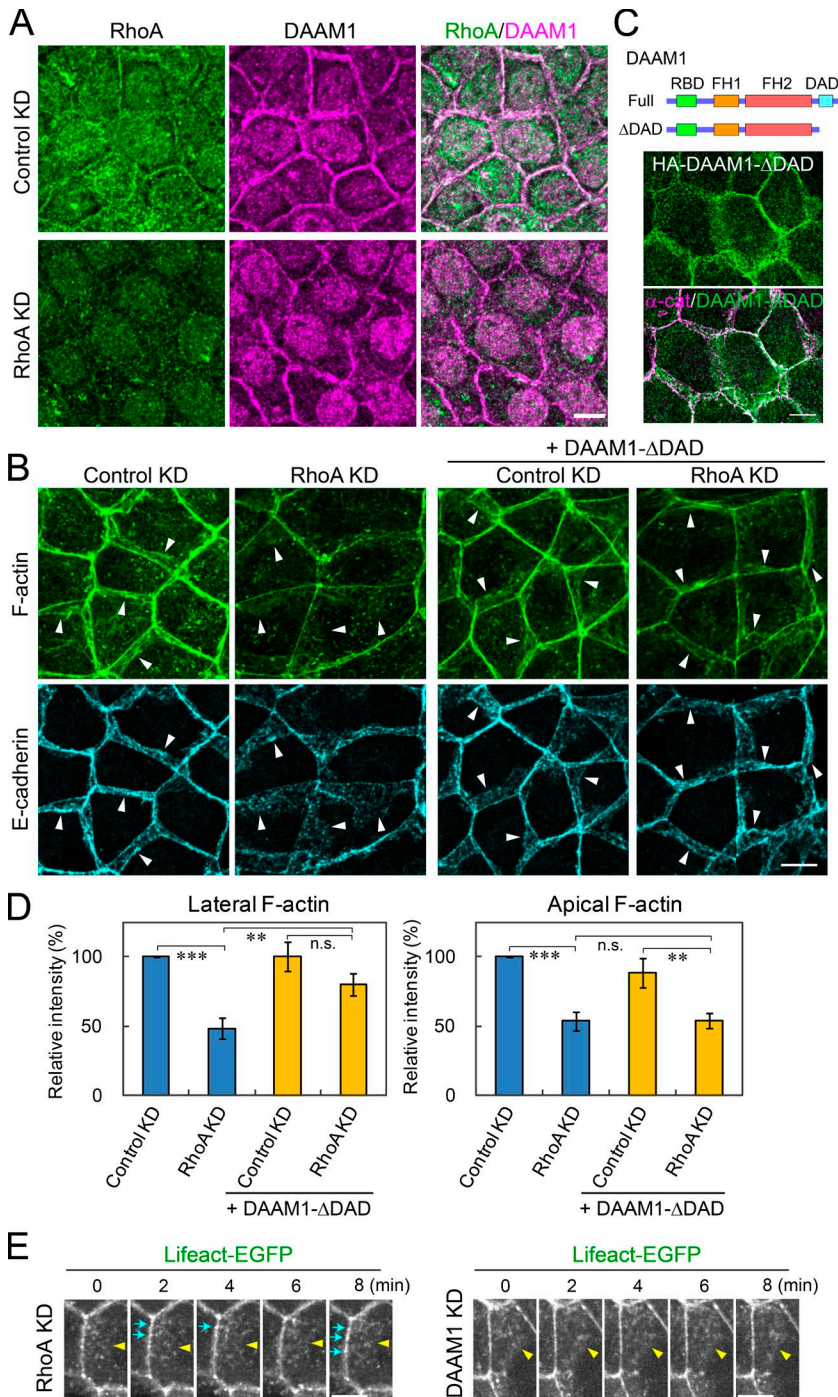
Figure 9. **RhoA regulates cell junctions upstream of DAAM1.** (A) Co-immunostaining for RhoA and DAAM1 in EpH4 cells treated with control or RhoA siRNA. Nuclear signals are caused by nonspecific reaction of the primary antibodies. (B) Effects of RhoA depletion and DAAM1-ΔDAD (shown in C) expression on junctional integrity. EpH4 cells or EpH4 cells stably expressing DAAM1-ΔDAD were treated with control or RhoA-specific siRNAs and co-stained for F-actin or E-cadherin. RhoA KD down-regulated not only the lateral but also apical F-actin, and DAAM1-ΔDAD expression restored a nearly normal level of lateral F-actin but not that of apical F-actin in Rho-depleted cells. Arrowheads point to the basal edges of the junctions. (C) The constitutively active DAAM1 mutant DAAM1-ΔDAD. (Top) Schematic representation of the mutant construct. (Bottom) Distribution of HA-tagged DAAM1-ΔDAD in EpH4 cells. α-cat, α-catenin. (D) Quantification of lateral and apical F-actin intensity in the experiments shown in B. Histograms represent the mean of three experiments. Error bars indicate SD. **, P < 0.01; ***, P < 0.001; n.s., not significant. (E) Still images of Video 9, in which Lifeact-EGFP–expressing cells were transfected with RhoA siRNA (left). The distribution of Lifeact-EGFP signals at the AJC changed dynamically. Blue arrows indicate examples of Lifeact-EGFP clusters that were only transiently detectable. Yellow arrowheads point to the basal edges of the junctions. For comparison, still images of Video 2, in which Lifeact-EGFP–expressing cells were transfected with DAAM1 siRNA, are also shown (right). Lifeact-EGFP signals were more stable in DAAM1-depleted than in RhoA-depleted cells at the AJC. (A–C and E) Bars, 10 µm.

D). These results are consistent with the idea that RhoA works upstream of DAAM1 to regulate lateral F-actin, although it also regulates apical F-actin via some effectors not identified here.

Discussion

Cell junctions are stably maintained in mature epithelial cells. When DAAM1 was depleted in EpH4 cells, however, the cell membranes forming LCs became mobile, similar to the leading edges of migrating cells. This enhancement of motility depended on the Rac–WRC signaling system, which is generally important for the formation of leading edges or lamellipodia in migrating cells (Krause and Gautreau, 2014). These results suggest that the membranes of LCs are motile by nature, like free cell edges, but this ability is normally restrained by DAAM1 (Fig. S5 F). Consistent with our observations, a previous study using DAAM1 gene trap mice showed that, in cardiomyocytes with a marked reduction of DAAM1, the distributions of F-actin, N-cadherin, and α-catenin were perturbed, leading to abnormal sarcomere organization and cell misalignment (Li et al., 2011).

DAAM1, as a member of the formin family, is thought to nucleate and/or accelerate the elongation of actin filaments. DAAM1 depletion induced fragmentation or diffusion of F-actin patches that are present in normal LCs. This suggests

that DAAM1-mediated actin polymerization is necessary to condense actin filaments at LCs. This view is supported by the recent observation that DAAM1 is required for maintaining the subcortical actin web in ciliated epithelial cells (Yasunaga et al., 2015). Our results also suggest that DAAM1 binds E-cadherin, and this binding is important for DAAM1 to localize to LCs, consistent with a previous finding that DAAM2, another formin related to DAAM1, binds the N-cadherin–α-catenin complex (Welsh et al., 2013). It is known that the CCC requires binding to F-actin via α-catenin for establishing firm cell–cell adhesion (Takeichi, 2014). Therefore, a role of DAAM1 at LCs might be to supply actin filaments to the CCC via physical association and to strengthen CCC-mediated intercellular junctions. Notably, although E-cadherin was up-regulated along the ZA, particularly in ZO-1/ZO-2 DKO cells, the DAAM1 level did not correlate with this up-regulation. Therefore, there must be a mechanism to suppress the interaction between DAAM1 and E-cadherin at the AJC.

How does DAAM1 interact with the Rac–WRC system for actin regulation? Here we propose two possible mechanisms: First, DAAM1 could actively inhibit the WRC or its downstream targets, but we failed to obtain evidence supporting this idea. Second, DAAM1 and the WRC might regulate F-actin independently, but in a conflicting manner. For example, DAAM1 might organize static actin networks to support CCC function, whereas the WRC accelerates actin dynamics, and their actions would be counterbalanced in normal junctions. Under this circumstance, removal of DAAM1 may allow the WRC to dominate actin regulation at LCs. Consistent with this idea, DAAM1 and WAVE2 appeared to localize in distinct microdomains. Testing these models is an important future subject.

Unlike the LCs, the AJC was hardly affected by DAAM1 loss, suggesting that F-actin organization at the AJC and LCs is controlled via distinct mechanisms. Nevertheless, our results suggest that they share RhoA as a common regulator. To receive Rho signals differentially, the AJC and LCs should have distinct Rho effectors. DAAM1 is likely to be one such Rho effector that predominantly serves at LCs.

Extrusion of tumor cells from the basal side of epithelial layers is thought to promote cancer invasion (Slattum and Rosenblatt, 2014). It has been suggested that DAAM1 depletion may be involved in the invasiveness of astrocytoma cells (Shu et al., 2011). Recent studies showed that Lamellipodin, whose action is negatively regulated by DAAM1 as shown in the present study, also promotes invasive cancer cell migration (Carmona et al., 2016). We found that, in prolonged cultures of DAAM1-depleted EpH4 cells, some of the cells began to relocate toward the basal sides. In spherical cultures of these cells, a fraction of cells tended to be extruded from the main body of the sphere, indicating that epithelial cells are unable to maintain robust tissue structures when DAMM1 is lost. Furthermore, DAAM1-depleted cells protruded long processes from LCs, especially when they were in contact with normal cells, suggesting that the interaction between DAAM1-depleted and normal cells promotes cell edge protrusion. Although the infiltration of cancer cells into the extracellular matrices is thought to be a major step in cancer metastasis, our results suggest that neoplastic cells may also be able to invade the boundaries between normal cells, when the motility of LCs is enhanced. It will be intriguing to investigate whether DAAM1 loss indeed serves as a mechanism to enhance cancer invasion and metastasis.

Materials and methods

Plasmids and siRNAs

An expression plasmid for HA-tagged mouse DAAM1 was described previously (Nishimura et al., 2012). Its deletion mutants were subcloned into a pCAH vector with a HA-tag attached to the N terminus. Point mutations of DAAM1 were introduced using a KOD-Plus Mutagenesis kit (TOYOBO). The plasmid for siRNA-resistant DAAM1 was prepared by introducing three silent mutations at the corresponding sequence to DAAM1 siRNA #1. To prepare the actin polymerization–deficient siRNA-resistant DAAM1 plasmid, an additional mutation, which changed I698 to A698, was further introduced (Jaiswal et al., 2013). EGFP-tagged mouse E-cadherin plasmid was described previously (Taguchi et al., 2011), and its insert was subcloned into a pCA-FLAG vector. Lifeact-EGFP (Riedl et al., 2008) plasmid was constructed by inserting its corresponding oligo DNA into a pCAH-EGFP vector. The plasmid for membrane EGFP was provided by N. Ueno (National Institute for Basic Biology, Okazaki, Aichi, Japan; Suzuki et al., 2010), and the insert was subcloned into a pCA vector. The plasmid for HA-tagged constitutively active Rac1 (G12V) was provided by Y. Nakaya (RIKEN Quantitative Biology Center, Suita, Osaka, Japan; Nakaya et al., 2004). The plasmid for HA-tagged wild-type and constitutively active RhoA (G14V) were provided by K. Kaibuchi (Nagoya University, Nagoya, Aichi, Japan; Amano et al., 1996). Dominant-negative RhoA (T19N) plasmid was prepared by introducing point mutations into the wild type.

Custom-synthesized siRNA oligos (Stealth RNAs) were purchased from Invitrogen, and the target sequences are as follows: mouse DAAM1 siRNA#1 and #2, 5′-GCCTGTCATGTATTCTCAACTTTCT-3′ and 5′-GAGTTCTACATTGATCAGCTCAATT-3′, respectively; mouse RhoA siRNA#1 and #2, 5′-CCATCAGGAAGAAACTGG TGATTGT-3′ and 5′-GAAGAAACTGGTGATTGTTGGTGAT-3′, respectively; mouse WAVE2 siRNA#1 and #2, 5′-GCAGGACACCAA GGATATCATGAAA-3′ and 5′-AGCGGGTTGACCGAGTACAAG TTAA-3′, respectively; mouse Lamellipodin siRNA, 5′-CAGCATGGA TTCTCTGGATATTGAT-3′; mouse ArpC3 siRNA, 5′-CCTGGCTTT CCTCTCAACGCCATTT-3′; and mouse E-cadherin siRNA, 5′-CCG ACCGGAAGTGACTCGAAATGAT-3′. Unless otherwise noted, we used siRNA#1 throughout the experiments. We used the Stealth RNAi siRNA Negative Control Medium GC Duplex #2 (12935-112; Invitrogen) as a control. For stable shRNA expression, a DNA oligo for DAAM1 siRNA#1 sequence was inserted into the pBASi-mU6-PUR vector (Takara Bio Inc.).

Antibodies and reagents

Rat anti–E-cadherin antibody clone ECCD2 (Shirayoshi et al., 1986), rat anti-Nap1 antibody (Nakao et al., 2008), and rabbit anti–Nectin-1α (Togashi et al., 2006) were described previously. The following antibodies were purchased: mouse anti-DAAM1 (for N terminus) and anti–pY150-WAVE2 (ECM Biosciences); rabbit anti-DAAM1 (for C terminus; Abgent); rabbit anti-DAAM1 (Proteintech); rabbit anti–α-catenin, rabbit anti–β-catenin, rabbit anti–l-afadin, rabbit myosin IIA/IIB, mouse anti–α-tubulin, and rabbit anti-FLAG (Sigma-Aldrich); mouse or rabbit anti–ZO-1 (Invitrogen); rabbit anti-WAVE2 and mouse anti–phosphorylated myosin light chain (Cell Signaling Technology); rabbit anti-lamellipodin (anti-RAPH1; Atlas); mouse anti-RhoA and rabbit anti–ZO-2 (Santa Cruz Biotechnology, Inc.); mouse anti-Abi1 (MBL); mouse anti-HA clone 16B12 and mouse anti-GST clone 4C10 (Covance); rat anti-HA clone 3F10 (Roche); Alexa Fluor–conjugated secondary antibodies (Molecular Probes); Alexa Fluor 647– or peroxidase-conjugated anti–rat IgG

(Jackson ImmunoResearch Laboratories, Inc.); CF488A-labeled anti–rat IgG (Biotium); and peroxidase-conjugated anti–mouse or anti–rabbit IgG (GE Healthcare). Rac inhibitor EHT-1864 was purchased from Tocris Bioscience. Arp2/3 inhibitor CK-666 was purchased from EMD Millipore.

Cell culture and transfection

EpH4 cells (López-Barahona et al., 1995; a gift of E. Reichmann, University of Zurich, Zurich, Switzerland) and HEK293T cells (RIKEN BioResource Center) were grown in a 1:1 mixture of DMEM and Ham's F12 medium (Wako Pure Chemical Industries) supplemented with 10% FBS (Nichirei Biosciences). Cells were transfected with plasmids for 1 d using Lipofectamine 2000 (Invitrogen). Stable transfectants were selected and maintained in a culture medium containing hygromycin B or puromycin (InvivoGen). For the expression of siRNAs, cells were transfected for 3 d using Lipofectamine RNAi-MAX (Invitrogen).

For long-term cultures, EpH4 cell lines stably expressing control or DAAM1 shRNA were seeded in the upper chamber of Transwell Permeable Supports (Coaster) and cultured for 2 wk, changing the medium every other day. For mixed cultures on collagen gels, cells precultured in 3.5-cm dishes were labeled with 10 µM CMTPX (Molecular Probes) in a serum-free medium at 37°C for 30 min. Then, the labeled cells were mixed with nonlabeled cells at a 1:50 ratio, seeded on cover glasses coated with 50 µl collagen-IA gel (Nitta Gelatin), which were placed in 24-well plates, and cultured for 2 d. For sphere cultures, cover glasses placed in 24-well plates were coated with 50 µl Matrigel Matrix (Corning). Then, cells were seeded on them in culture medium containing 2% Matrigel Matrix and cultured for 6 d, changing the medium every day.

Double knockout of ZO-1 and ZO-2 genes

An EpH4 cell line, in which the ZO-1 genes were knocked out, was established by conventional homologous recombination (Umeda et al., 2006). Then, this clone was used to further knock out the ZO-2 genes using the CRISPR-Cas9 system. Oligonucleotides were phosphorylated, annealed, and cloned into the BsmBI site of pLenti-CRISPR v2 vector according to the Zhang laboratory protocols (F. Zhang, MIT, Cambridge, MA). The target sequence for mouse ZO-2 was 5′-GCTTATGAACCCGACTACGG-3′.

Immunofluorescence staining of cells

Cells grown on cover glasses were fixed with 1% (wt/vol) PFA in the medium at RT for 10 min. In the case of sphere cultures, 2% (wt/vol) PFA was used for fixation. Cells were made permeable with 0.5% Triton X-100 in TBS for 20 min. The samples were blocked with 3% (wt/vol) BSA and 10% (vol/vol) goat serum in TBS containing 0.1% Triton X-100 (TBS-T) and incubated with primary antibodies in the Can Get Signal immunostain solution (TOYOBO) at RT for 2 h. After washes, the cells were incubated with fluorescence-labeled secondary antibodies for 1 h. After further washes, cells were incubated with fluorescence-labeled phalloidin (Molecular Probes) for 30 min and subsequently mounted using FluoroSave (EMD Millipore). Images of cells were obtained using a laser-scanning confocal microscope LSM710/780 (ZEISS) equipped with an αPlan-FLUAR 100×/1.45 oil lens or Plan-Apochromat 63×/1.40 oil lens (ZEISS) at RT. Z-stack images were taken at every 0.3 µm. For observation of the lateral views with higher resolution, images were obtained by the laser-scanning confocal microscope LSM880-Airyscan (ZEISS) equipped with an αPlan-FLUAR 100×/1.45 oil lens at RT. Z-stack images were taken at every 0.17 µm and subjected to Airyscan super-resolution mode processing. Images were processed using ZEN software (ZEISS) and Photoshop CS5 (Adobe Systems).

Immunoprecipitation and GST pull-down

For immunoprecipitation using HA-DAAM1–expressing cells, cells were lysed at 4°C for 20 min in a lysis buffer consisting of 50 mM Tris-HCl, pH 7.5, 1% Nonidet P-40, 150 mM NaCl, 10 mM $MgCl_2$, and a protease inhibitor cocktail (Roche). After centrifugation, supernatants were incubated with anti-HA clone 3F10 affinity beads (Roche) at 4°C for 2 h. After washing the beads, bound proteins were subjected to SDS-PAGE and then Western blotting. Signals on the blots were detected using the Western Blotting Substrate Plus detection system (Thermo Fisher Scientific). In the case of mass spectrometry analysis, immunoprecipitated proteins were eluted using HA peptides (Babco), reprecipitated by TCA, and analyzed by silver staining (silver stain MS kit; Wako Pure Chemical Industries). To immunoprecipitate endogenous DAAM1, EpH4 cells were lysed in a lysis buffer consisting of 50 mM Tris-HCl, pH 7.5, 1% Triton X-100, 0.02% SDS, 0.5% deoxycholate, 150 mM NaCl, 10 mM $MgCl_2$, and a protease inhibitor cocktail. The supernatant was incubated with either anti-DAAM antibody (Proteintech) or normal rabbit IgG (Santa Cruz Biotechnologies, Inc.) and then with Protein G–Sepharose (GE Healthcare).

For GST pull-down assays, HA-tagged DAAM1-N cell lysate was incubated with purified GST-tagged E-cadherin cytoplasmic region (aa 734–884), β-catenin, α-catenin, or GST alone for 1.5 h and then with Glutathione–Sepharose 4B (GE Healthcare). GST pull-down for active Rac1 was performed using a Rac1/Cdc42 activation assay kit (EMD Millipore).

Time-lapse imaging

Cells expressing Lifeact-EGFP or E-cadherin–EGFP were transfected with siRNAs and cultured in glass-bottom dishes (IWAKI) for 3 d. In the case of membrane-EGFP imaging in DAAM1-depleted cell lines, cells were seeded on glass-bottom dishes coated with 200 µl collagen-IA gel, transfected with membrane-EGFP on the next day, and cultured for one more day. Time-lapse imaging was performed using a spinning-disc laser confocal microscope IX71 (Olympus) equipped with CSU-X1 (Yokogawa Electric Corporation) and with an UplanSApo 60×/1.35 oil lens or a LUCPlanFLN 60×/0.70 lens (Olympus) in 5% CO_2 at 37°C. Z-stack images were taken every 2 or 5 min. Images were processed using MetaMorph software (Molecular Devices) and ImageJ software (National Institutes of Health).

Quantification of junctions

Fluorescence intensity as well as the area or length of objects in photographic images were measured using ImageJ software. Lateral F-actin intensity was quantified as follows: Using Z-projected E-cadherin images, the LC region was first outlined. Next, using the F-actin channel of the same images, cytoplasmic background intensity was subtracted, and then the mean gray value per pixel at the LC region was measured. Apical F-actin intensity was quantified by drawing a line along AJC using the background-subtracted F-actin images and then by measuring the mean gray value on this line. The degree of tilting of LCs was quantified as follows: LC area was defined as above. Then, the width of the border between the LC and AJC areas was measured. Subsequently, the LC area was divided by the width of the border to obtain a mean LC area per AJC unit (1 µm). This value was defined as the "tilting extent." Quantifications were performed for 50–100 junctions from four microscopic fields in each experiment. For the mixed culture experiments, 25–80 cells from four microscopic fields were quantified for protrusion number and length in each experiment. For the sphere culture experiments, 13–16 spheres were quantified for cell extrusion in each experiment. Mean and SD were calculated from three separate experiments. Statistical analyses were performed using R software (The R Foundation).

Online supplemental material

Fig. S1 shows a summary of mass spectrometry analysis, DAAM1 siRNA efficiencies, and the distribution of junctional proteins in control and DAAM1-depleted cells. Fig. S2 shows characteristics of the ZO-1/ZO-2 DKO EpH4 cell line and the effect of DAAM1 KD on this line. Fig. S3 shows the effects of the expression of a siRNA-resistant DAAM1, as well as its mutant that is unable to support actin polymerization, in DAAM1-depleted cells. Fig. S4 shows Western blot analysis of DAAM1-depleted stable lines and active Rac pull-down assay of these cells; the effects of a Rac inhibitor and the expression of a constitutively active Rac1 mutant on lateral contacts are also shown; distribution of WAVE complex components and the Western blotting analysis of WAVE2 siRNA efficiency are also provided. Fig. S5 shows analyses of the cells treated with siRNAs specific for lamellipodin, ArpC3, and RhoA; a schematic summary of the lateral contact regulation by DAAM1 and WRC is also shown. Videos 1 and 2 show F-actin dynamics in control and DAAM1-depleted EpH4 cells. Videos 3 and 4 show E-cadherin dynamics in control and DAAM1-depleted EpH4 cells. Videos 5 and 6 show movement of cell membranes in control and DAAM-depleted EpH4 cells. Video 7 shows E-cadherin dynamics in DAAM1-depleted EpH4 cells treated with a Rac inhibitor. Video 8 shows E-cadherin dynamics in EpH4 cells simultaneously transfected with DAAM1 and WAVE2 siRNAs. Videos 9 and 10 show F-actin and E-cadherin dynamics in RhoA-depleted EpH4 cells.

References

Amano, M., H. Mukai, Y. Ono, K. Chihara, T. Matsui, Y. Hamajima, K. Okawa, A. Iwamatsu, and K. Kaibuchi. 1996. Identification of a putative target for Rho as the serine-threonine kinase protein kinase N. *Science.* 271:648–650. http://dx.doi.org/10.1126/science.271.5249.648

Ang, S.F., Z.S. Zhao, L. Lim, and E. Manser. 2010. DAAM1 is a formin required for centrosome re-orientation during cell migration. *PLoS One.* 5:e13064. http://dx.doi.org/10.1371/journal.pone.0013064

Carmona, G., U. Perera, C. Gillett, A. Naba, A.L. Law, V.P. Sharma, J. Wang, J. Wyckoff, M. Balsamo, F. Mosis, et al. 2016. Lamellipodin promotes invasive 3D cancer cell migration via regulated interactions with Ena/VASP and SCAR/WAVE. *Oncogene.* 35:5155–5169. http://dx.doi.org/10.1038/onc.2016.47

Carramusa, L., C. Ballestrem, Y. Zilberman, and A.D. Bershadsky. 2007. Mammalian diaphanous-related formin Dia1 controls the organization of E-cadherin-mediated cell-cell junctions. *J. Cell Sci.* 120:3870–3882. http://dx.doi.org/10.1242/jcs.014365

Chesarone, M.A., A.G. DuPage, and B.L. Goode. 2010. Unleashing formins to remodel the actin and microtubule cytoskeletons. *Nat. Rev. Mol. Cell Biol.* 11:62–74. http://dx.doi.org/10.1038/nrm2816

Etienne-Manneville, S. 2008. Polarity proteins in migration and invasion. *Oncogene.* 27:6970–6980. http://dx.doi.org/10.1038/onc.2008.347

Fanning, A.S., C.M. Van Itallie, and J.M. Anderson. 2012. Zonula occludens-1 and -2 regulate apical cell structure and the zonula adherens cytoskeleton in polarized epithelia. *Mol. Biol. Cell.* 23:577–590. http://dx.doi.org/10.1091/mbc.E11-09-0791

Farquhar, M.G., and G.E. Palade. 1963. Junctional complexes in various epithelia. *J. Cell Biol.* 17:375–412. http://dx.doi.org/10.1083/jcb.17.2.375

Grikscheit, K., T. Frank, Y. Wang, and R. Grosse. 2015. Junctional actin assembly is mediated by Formin-like 2 downstream of Rac1. *J. Cell Biol.* 209:367–376. http://dx.doi.org/10.1083/jcb.201412015

Gupta, G.P., and J. Massagué. 2006. Cancer metastasis: building a framework. *Cell.* 127:679–695. http://dx.doi.org/10.1016/j.cell.2006.11.001

Habas, R., Y. Kato, and X. He. 2001. Wnt/Frizzled activation of Rho regulates vertebrate gastrulation and requires a novel Formin homology protein Daam1. *Cell.* 107:843–854. http://dx.doi.org/10.1016/S0092-8674(01)00614-6

Higashi, T., T. Ikeda, R. Shirakawa, H. Kondo, M. Kawato, M. Horiguchi, T. Okuda, K. Okawa, S. Fukai, O. Nureki, et al. 2008. Biochemical characterization of the Rho GTPase-regulated actin assembly by diaphanous-related formins, mDia1 and Daam1, in platelets. *J. Biol. Chem.* 283:8746–8755. http://dx.doi.org/10.1074/jbc.M707839200

Hogan, C., S. Dupré-Crochet, M. Norman, M. Kajita, C. Zimmermann, A.E. Pelling, E. Piddini, L.A. Baena-López, J.P. Vincent, Y. Itoh, et al. 2009. Characterization of the interface between normal and transformed epithelial cells. *Nat. Cell Biol.* 11:460–467. http://dx.doi.org/10.1038/ncb1853

Jaiswal, R., D. Breitsprecher, A. Collins, I.R. Corrêa Jr., M.Q. Xu, and B.L. Goode. 2013. The formin Daam1 and fascin directly collaborate to promote filopodia formation. *Curr. Biol.* 23:1373–1379. http://dx.doi.org/10.1016/j.cub.2013.06.013

Ju, R., P. Cirone, S. Lin, H. Griesbach, D.C. Slusarski, and C.M. Crews. 2010. Activation of the planar cell polarity formin DAAM1 leads to inhibition of endothelial cell proliferation, migration, and angiogenesis. *Proc. Natl. Acad. Sci. USA.* 107:6906–6911. http://dx.doi.org/10.1073/pnas.1001075107

Kametani, Y., and M. Takeichi. 2007. Basal-to-apical cadherin flow at cell junctions. *Nat. Cell Biol.* 9:92–98. http://dx.doi.org/10.1038/ncb1520

Kobielak, A., H.A. Pasolli, and E. Fuchs. 2004. Mammalian formin-1 participates in adherens junctions and polymerization of linear actin cables. *Nat. Cell Biol.* 6:21–30. http://dx.doi.org/10.1038/ncb1075

Krause, M., and A. Gautreau. 2014. Steering cell migration: lamellipodium dynamics and the regulation of directional persistence. *Nat. Rev. Mol. Cell Biol.* 15:577–590. http://dx.doi.org/10.1038/nrm3861

Law, A.L., A. Vehlow, M. Kotini, L. Dodgson, D. Soong, E. Theveneau, C. Bodo, E. Taylor, C. Navarro, U. Perera, et al. 2013. Lamellipodin and the Scar/WAVE complex cooperate to promote cell migration in vivo. *J. Cell Biol.* 203:673–689. http://dx.doi.org/10.1083/jcb.201304051

Leng, Y., J. Zhang, K. Badour, E. Arpaia, S. Freeman, P. Cheung, M. Siu, and K. Siminovitch. 2005. Abelson-interactor-1 promotes WAVE2 membrane translocation and Abelson-mediated tyrosine phosphorylation required for WAVE2 activation. *Proc. Natl. Acad. Sci. USA.* 102:1098–1103. http://dx.doi.org/10.1073/pnas.0409120102

Li, D., M.A. Hallett, W. Zhu, M. Rubart, Y. Liu, Z. Yang, H. Chen, L.S. Haneline, R.J. Chan, R.J. Schwartz, et al. 2011. Dishevelled-associated activator of morphogenesis 1 (Daam1) is required for heart morphogenesis. *Development.* 138:303–315. http://dx.doi.org/10.1242/dev.055566

Liu, W., A. Sato, D. Khadka, R. Bharti, H. Diaz, L.W. Runnels, and R. Habas. 2008. Mechanism of activation of the Formin protein Daam1. *Proc. Natl. Acad. Sci. USA.* 105:210–215. http://dx.doi.org/10.1073/pnas.0707277105

López-Barahona, M., I. Fialka, J.M. González-Sancho, M. Asunción, M. González, T. Iglesias, J. Bernal, H. Beug, and A. Muñoz. 1995. Thyroid hormone regulates stromelysin expression, protease secretion and the morphogenetic potential of normal polarized mammary epithelial cells. *EMBO J.* 14:1145–1155.

Mandai, K., Y. Rikitake, M. Mori, and Y. Takai. 2015. Nectins and nectin-like molecules in development and disease. *Curr. Top. Dev. Biol.* 112:197–231. http://dx.doi.org/10.1016/bs.ctdb.2014.11.019

Martin, A.C., and B. Goldstein. 2014. Apical constriction: themes and variations on a cellular mechanism driving morphogenesis. *Development.* 141:1987–1998. http://dx.doi.org/10.1242/dev.102228

Mendoza, M.C., E.E. Er, W. Zhang, B.A. Ballif, H.L. Elliott, G. Danuser, and J. Blenis. 2011. ERK-MAPK drives lamellipodia protrusion by activating the WAVE2 regulatory complex. *Mol. Cell.* 41:661–671. http://dx.doi.org/10.1016/j.molcel.2011.02.031

Murphy, D.A., and S.A. Courtneidge. 2011. The 'ins' and 'outs' of podosomes and invadopodia: characteristics, formation and function. *Nat. Rev. Mol. Cell Biol.* 12:413–426. http://dx.doi.org/10.1038/nrm3141

Nakao, S., A. Platek, S. Hirano, and M. Takeichi. 2008. Contact-dependent promotion of cell migration by the OL-protocadherin-Nap1 interaction. *J. Cell Biol.* 182:395–410. http://dx.doi.org/10.1083/jcb.200802069

Nakaya, Y., S. Kuroda, Y.T. Katagiri, K. Kaibuchi, and Y. Takahashi. 2004. Mesenchymal-epithelial transition during somitic segmentation is regulated by differential roles of Cdc42 and Rac1. *Dev. Cell.* 7:425–438. http://dx.doi.org/10.1016/j.devcel.2004.08.003

Nishimura, T., H. Honda, and M. Takeichi. 2012. Planar cell polarity links axes of spatial dynamics in neural-tube closure. *Cell.* 149:1084–1097. http://dx.doi.org/10.1016/j.cell.2012.04.021

Ridley, A.J. 2011. Life at the leading edge. *Cell.* 145:1012–1022. http://dx.doi.org/10.1016/j.cell.2011.06.010

Riedl, J., A.H. Crevenna, K. Kessenbrock, J.H. Yu, D. Neukirchen, M. Bista, F. Bradke, D. Jenne, T.A. Holak, Z. Werb, et al. 2008. Lifeact: a versatile marker to visualize F-actin. *Nat. Methods.* 5:605–607. http://dx.doi.org/10.1038/nmeth.1220

Rotty, J.D., C. Wu, and J.E. Bear. 2013. New insights into the regulation and cellular functions of the ARP2/3 complex. *Nat. Rev. Mol. Cell Biol.* 14:7–12. http://dx.doi.org/10.1038/nrm3492

Shirayoshi, Y., A. Nose, K. Iwasaki, and M. Takeichi. 1986. N-linked oligosaccharides are not involved in the function of a cell-cell binding glycoprotein E-cadherin. *Cell Struct. Funct.* 11:245–252. http://dx.doi.org/10.1247/csf.11.245

Shu, M., X. Zheng, S. Wu, H. Lu, T. Leng, W. Zhu, Y. Zhou, Y. Ou, X. Lin, Y. Lin, et al. 2011. Targeting oncogenic miR-335 inhibits growth and invasion of malignant astrocytoma cells. *Mol. Cancer.* 10:59. http://dx.doi.org/10.1186/1476-4598-10-59

Slattum, G.M., and J. Rosenblatt. 2014. Tumour cell invasion: an emerging role for basal epithelial cell extrusion. *Nat. Rev. Cancer.* 14:495–501. http://dx.doi.org/10.1038/nrc3767

Suzuki, M., Y. Hara, C. Takagi, T.S. Yamamoto, and N. Ueno. 2010. MID1 and MID2 are required for *Xenopus* neural tube closure through the regulation of microtubule organization. *Development.* 137:2329–2339. http://dx.doi.org/10.1242/dev.048769

Taguchi, K., T. Ishiuchi, and M. Takeichi. 2011. Mechanosensitive EPL IN-dependent remodeling of adherens junctions regulates epithelial reshaping. *J. Cell Biol.* 194:643–656. http://dx.doi.org/10.1083/jcb.201104124

Takeichi, M. 2014. Dynamic contacts: rearranging adherens junctions to drive epithelial remodelling. *Nat. Rev. Mol. Cell Biol.* 15:397–410. http://dx.doi.org/10.1038/nrm3802

Takenawa, T., and S. Suetsugu. 2007. The WASP-WAVE protein network: connecting the membrane to the cytoskeleton. *Nat. Rev. Mol. Cell Biol.* 8:37–48. http://dx.doi.org/10.1038/nrm2069

Togashi, H., J. Miyoshi, T. Honda, T. Sakisaka, Y. Takai, and M. Takeichi. 2006. Interneurite affinity is regulated by heterophilic nectin interactions in concert with the cadherin machinery. *J. Cell Biol.* 174:141–151. http://dx.doi.org/10.1083/jcb.200601089

Umeda, K., J. Ikenouchi, S. Katahira-Tayama, K. Furuse, H. Sasaki, M. Nakayama, T. Matsui, S. Tsukita, M. Furuse, and S. Tsukita. 2006. ZO-1 and ZO-2 independently determine where claudins are polymerized in tight-junction strand formation. *Cell.* 126:741–754. http://dx.doi.org/10.1016/j.cell.2006.06.043

Verma, S., A.M. Shewan, J.A. Scott, F.M. Helwani, N.R. den Elzen, H. Miki, T. Takenawa, and A.S. Yap. 2004. Arp2/3 activity is necessary for efficient formation of E-cadherin adhesive contacts. *J. Biol. Chem.* 279:34062–34070. http://dx.doi.org/10.1074/jbc.M404814200

Verma, S., S.P. Han, M. Michael, G.A. Gomez, Z. Yang, R.D. Teasdale, A. Ratheesh, E.M. Kovacs, R.G. Ali, and A.S. Yap. 2012. A WAVE2-Arp2/3 actin nucleator apparatus supports junctional tension at the epithelial zonula adherens. *Mol. Biol. Cell.* 23:4601–4610. http://dx.doi.org/10.1091/mbc.E12-08-0574

Vogelmann, R., and W.J. Nelson. 2005. Fractionation of the epithelial apical junctional complex: reassessment of protein distributions in different substructures. *Mol. Biol. Cell.* 16:701–716. http://dx.doi.org/10.1091/mbc.E04-09-0827

Walck-Shannon, E., and J. Hardin. 2014. Cell intercalation from top to bottom. *Nat. Rev. Mol. Cell Biol.* 15:34–48. http://dx.doi.org/10.1038/nrm3723

Welsh, I.C., M. Thomsen, D.W. Gludish, C. Alfonso-Parra, Y. Bai, J.F. Martin, and N.A. Kurpios. 2013. Integration of left-right Pitx2 transcription and Wnt signaling drives asymmetric gut morphogenesis via Daam2. *Dev. Cell.* 26:629–644. http://dx.doi.org/10.1016/j.devcel.2013.07.019

Wu, S.K., G.A. Gomez, M. Michael, S. Verma, H.L. Cox, J.G. Lefevre, R.G. Parton, N.A. Hamilton, Z. Neufeld, and A.S. Yap. 2014. Cortical F-actin stabilization generates apical-lateral patterns of junctional contractility that integrate cells into epithelia. *Nat. Cell Biol.* 16:167–178. http://dx.doi.org/10.1038/ncb2900

Yamazaki, D., T. Oikawa, and T. Takenawa. 2007. Rac-WAVE-mediated actin reorganization is required for organization and maintenance of cell-cell adhesion. *J. Cell Sci.* 120:86–100. http://dx.doi.org/10.1242/jcs.03311

Yang, J., and R.A. Weinberg. 2008. Epithelial-mesenchymal transition: at the crossroads of development and tumor metastasis. *Dev. Cell.* 14:818–829. http://dx.doi.org/10.1016/j.devcel.2008.05.009

Yasunaga, T., S. Hoff, C. Schell, M. Helmstädter, O. Kretz, S. Kuechlin, T.A. Yakulov, C. Engel, B. Müller, R. Bensch, et al. 2015. The polarity protein Inturned links NPHP4 to Daam1 to control the subapical actin network in multiciliated cells. *J. Cell Biol.* 211:963–973. http://dx.doi.org/10.1083/jcb.201502043